PHYSICAL REVIEW B VOLUME 13, NUMBER 7 1 APRIL 1976

Vibrational-mode shifts in inelastic electron tunneling spectroscopy: Effects due to superconductivity and surface interactions*

John Kirtley and Paul K. Hansma
Department of Physics, University of California, Santa Barbara, California 93106
(Received 22 September 1975)

Measurements of the effect of the top metal electrode on the vibrational-mode energies of benzoic acid on aluminum oxide with Pb, Sn, and Ag top metal electrodes are described. Peak shifts of approximately 15 meV for the O-H stretch modes of hydroxyl ions, 0.5 meV for the C-H bending modes, and less than 0.2 meV for the C-C ring stretch and bend modes of benzoate molecules were found. These measurements are discussed in terms of a simple image model. For junctions with superconducting electrodes a modulation-dependent correction must be made to the measured peak positions. A theory is developed for the line shapes and peak positions of both the second and third harmonic signals and compared with experiment.

I. INTRODUCTION

Several years ago Drexhage, Kuhn, and Schaefer[1] observed a distance-dependent modulation of the fluorescence decay time of monomolecular layers of Eu^{3+} ions at well-controlled distances (down to 20 Å) from a metal mirror. Morawitz[2] analyzed this effect in terms of an image theory, predicting spatial modulation in the transition frequency and width of the excited state of the ions owing to a resonance interaction with the radiation field reflected from the mirror. Kuhn[3] generalized the calculations to the case of a non-perfectly-conducting surface. Barton,[4] Philpott,[5] and Milonni and Knight[6] considered the decay of an excited atom between two infinite mirrors. The theory has been extended to include nonresonant coupling to surface waves by Tews[7] and Chance, Prock, and Silbey.[8] Morawitz and Philpott[9] emphasized the case of resonance coupling to surface plasmons.

In a recent paper[10] we described experiments similar to those of Drexhage *et al.*,[1] but in an entirely different regime. In that work we studied the effect of different top metal electrodes on the vibrational stretching modes of hydroxyl and deuteroxyl ions adsorbed on aluminum-oxide and magnesium-oxide surfaces, using inelastic electron tunneling spectroscopy. Although working at infrared rather than visible frequencies, with vibrational rather than electronic transitions, and with a top metal surface in direct contact with the adsorbed molecules, we found that an image theory closely resembling that of Morawitz[2] could be used to model our experiments.

We report in this paper experiments which extend the study of the effect of the top metal electrode on vibrational modes in inelastic electron tunneling spectroscopy (IETS) to a variety of vibrational modes of a larger molecule, benzoic acid. This study was undertaken for two reasons: (i) The effect of the top metal electrode on the IETS spectra of molecules must be understood in order to make comparisons between IETS data (with a top metal electrode) and Raman and infrared data (without a top electrode); and (ii) The wider variety of vibrational modes available for study with benzoic acid allow a more stringent test of any model for the effect of the top metal electrode in IETS.

Our experiments showed that in comparison to the shifts due to the top metal electrode for hydroxyl ions, which were as large as 22 meV, the shifts for the C-H bond modes in benzoic acid on alumina[11] were less than 1 meV, and those for the C-C ring modes were less than 0.2 meV. These results can be understood in terms of an image dipole model. The relatively small shifts observed for benzoic acid on alumina are encouraging with respect to the comparison of electron tunneling with optical data.

In the course of our work we have also found that the observed peak energies in IETS are not shifted out by the full gap energy of the superconducting electrodes. We include in this paper a model for the effect of superconducting electrodes on the observed peak energies and compare this model with experiment.

II. EXPERIMENTAL TECHNIQUES

Our samples were prepared by evaporating a 2000-Å thick layer of aluminum through a mask onto a glass microscope slide at a pressure of less than 5×10^{-5} Torr, exposing the films to air for approximately 30 sec to form a thin oxide layer, liquid doping with a 0.5-mg/ml solution of benzoic acid in water, and returning the slides to

the vacuum chamber for evaporation of the top metal electrode. The substrates were cooled to liquid-nitrogen temperature before completing the junctions. A more detailed description of our general sample-preparation and evaluation techniques has been previously published.[10,12]

Samples were run at 4.2 °K by simply inserting them into a standard helium storage Dewar. For experiments requiring lower temperature or a magnetic field to quench superconductivity the samples were run in a conventional pumped helium research Dewar equipped with a 30-kOe superconducting solenoid. Spectra were obtained from good samples[13] by applying a small alternating modulation current in addition to a slowly sweeping bias current through the junction, measuring the dc component of the resulting voltage across the junction with a PAR 113 preamplifier feeding into the x axis of an xy chart recorder, and measuring the second or third harmonic components of this voltage with a PAR 124 lock-in amplifier feeding into the y axis of the chart recorder. Spectra for the second and third harmonic voltages for Al-oxide-benzoic-acid-Pb samples at 1.1 °K are shown in Fig. 1. Details on the techniques for measuring the second harmonic spectra have been published. Since this is, however, the first reported use of third harmonic spectra for IETS, to our knowledge, more detail is in order. We obtained the reference signal for the lock-in amplifier by running the modulation voltage through a frequency tripler (circuit diagram available on request). The lock-in amplifier was then run in the external reference mode. It was important that the modulation signal be free of third harmonic distortion to better than 0.01%. We found a Krohn-Hite Model 4000 operating at 1120 Hz to be adequate; most oscillators, however, require a notch filter at the third harmonic frequency on the output.

It could be expected that the third harmonic signal might be orders of magnitude smaller than the second. (The second is of order 10^{-3} times the first.) Fortunately, this is note the case; the third is, in general, less than one order of magnitude smaller than the second. The advantages of measuring the third harmonic spectra were that the background signal was smaller (see Fig. 1); and it was possible to get greater accuracy in the determination of mode energies, since the voltage of the zero crossing in the third derivative could be measured more precisely than the voltage of the top of the peak in the second derivative.

For accurate measurement of the mode energies the peaks were measured point by point. We adjusted the bias current with a 40-turn single-filament potentiometer used as a voltage divider, and we measured the bias voltage with an L- and N-type K3 potentiometer. All voltages were calibrated through the potentiometer to a standard cell. The output voltage of the lock-in amplifier, which had a 30 sec time constant, was measured with a digital voltmeter.

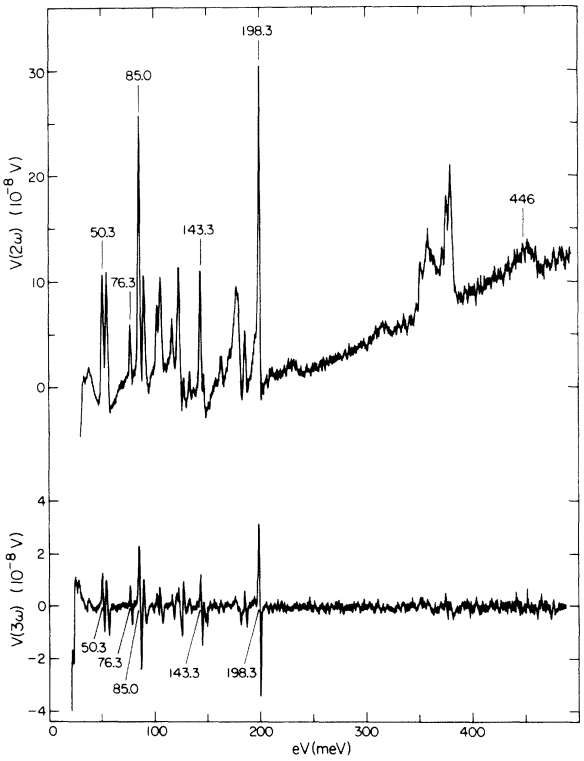

FIG. 1. Inelastic electron tunneling second (top) and third (bottom) harmonic spectra for an Al–Al-oxide–benzoic-acid–Pb tunneling junction, taken at 1.1 °K with a 1-mV modulation voltage. The labeled peaks are those chosen for study and discussed in the text. The second harmonic spectra corresponds to a second derivative of the current-voltage characteristic, and the third harmonic corresponds to a third derivative. Notice that a peak maximum in the second harmonic signal corresponds to a zero crossing in the third harmonic. The third harmonic, while smaller in amplitude than the second, has little background and enables greater accuracy in mode energy measurements.

III. EFFECT OF SUPERCONDUCTIVITY

Figure 2 shows a comparison of the second harmonic signals for the 198.3-meV C-C stretch mode of benzoic acid on alumina with a Pb top electrode with and without a magnetic field to quench superconductivity. Also shown is the second harmonic signal for the same mode with an Ag top electrode. All measurements were at

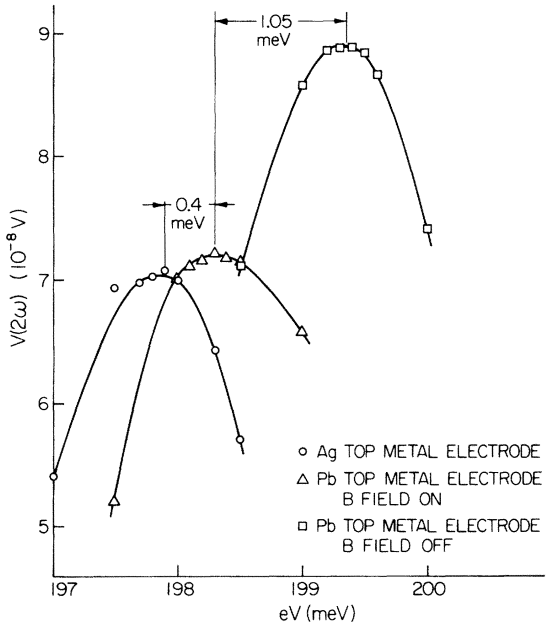

FIG. 2. Plot of second harmonic signal of the 198.3-meV mode of benzoic acid on alumina for Ag top electrode and a Pb top electrode with and without a magnetic field to quench the superconductivity, taken at 1.1 °K with a 1-mV modulation voltage. The peak maximum is shifted by 0.4 meV for the quenched Pb with respect to the Ag, and by 1.05 meV for the superconducting Pb with respect to the normal Pb. The combined gap $\Delta_{Al}+\Delta_{Pb}$ for this sample was 1.45 meV; therefore the peak did not shift out by the full energy gap when the junction became superconducting.

1.1° K with a 1-mV modulation voltage. For the Pb top electrode, the peak shifted out by 1.05 mV when the lead and aluminum electrodes were superconducting; but the combined gap $\Delta_{Al}+\Delta_{Pb}$, as measured from the elastic I-V characteristic of the junction, was 1.45 meV. Thus the peak did not shift out by the full gap energy.[15]

This effect can be understood qualitatively as follows: For a normal metal junction at low temperatures with a vibrational mode of frequency ω_0, inelastic electron tunneling current will flow when the junction is biased at a voltage V such that $eV \geq \hbar\omega_0$. This extra current causes a very small increase in the slope of the current-voltage characteristic of the junction at $eV=\hbar\omega_0$. The increase in slope becomes a step when one derivative of the I-V characteristic is taken, and the step becomes a peak for plots of d^2I/dV^2 vs V. When an electrode becomes superconducting a forbidden-energy region develops, and inelastic tunneling current cannot flow until $eV \geq \hbar\omega_0+\Delta$, where 2Δ is the energy gap. Because of the bunching of the BCS density of states around the band edge, the inelastic current approaches asymptotically the value it would have had if the electrode was normal as the bias voltage is increased. Rather than a small change in slope at $eV=\hbar\omega_0$, there is a larger increase in slope at $eV=\hbar\omega_0+\Delta$ plus a concave downward portion of the I-V characteristic for $eV>\hbar\omega_0+\Delta$, approaching the characteristic the junction would have had if the films were normal as the bias voltage gets large. The second harmonic signal at a given bias voltage is proportional to the curvature of the total current-voltage characteristic averaged over the voltage modulation interval. Therefore the negative curvature of the I-V characteristic for $eV> \hbar\omega_0+\Delta$ pulls down the high-voltage side of the second derivative peak, shifting the position of the peak maximum down in voltage. Since the modulation voltages are comparable to the gap energies, the observed shifts are not negligible when compared with the gap energies. Larger modulation voltages produce larger discrepancies. (No modulation-voltage dependence of the measured peak positions was found when the electrodes were normal.)

To model the effect quantitatively we write the inelastic tunneling current as[16]

$$I_i(eV)=k\int_0^\infty d\omega\, D(\omega)\int_{-\infty}^{\infty} dE\, f(E) \times[1-f(E+eV-\hbar\omega)]N_1(E)N_2(E+eV-\hbar\omega), \tag{1}$$

where N_1 and N_2 are the effective tunneling densities of states on either side of the tunneling barrier, $f(E)$ is the Fermi-Dirac distribution of filled states, and $D(\omega)$ is the distribution of oscillator strengths. The observed second harmonic signal is given by[17]

$$I_{2\omega}(eV_0)=\frac{2}{\tau}\int_0^\tau dt\, I_i(eV_0+eV_\omega\cos\omega t)\cos 2\omega t, \tag{2}$$

where V_0 is the constant bias voltage and V_ω is the modulation voltage. An analogous equation for the third harmonic signal can be written by replacing $\cos(2\omega t)$ by $\cos(3\omega t)$. We set N_1 and N_2 equal to the BCS density of states,[18] assumed a Gaussian spectral line shape, [19]

$$D(\omega)=2(\alpha/\pi)^{1/2}e^{-\alpha(\omega-\omega_0)^2},$$

and integrated Eqs. (1) and (2) numerically on a PDP 15 computer.[20] Figure 3 compares the experimental and theoretical line shapes for the 198.3-meV line of benzoic acid with a lead top electrode at 1.1° K for the second and third harmonic signals for three different modulation voltages. (Since the lock-in amplifier reads rms voltages, a modulation voltage of 1 mV corre-

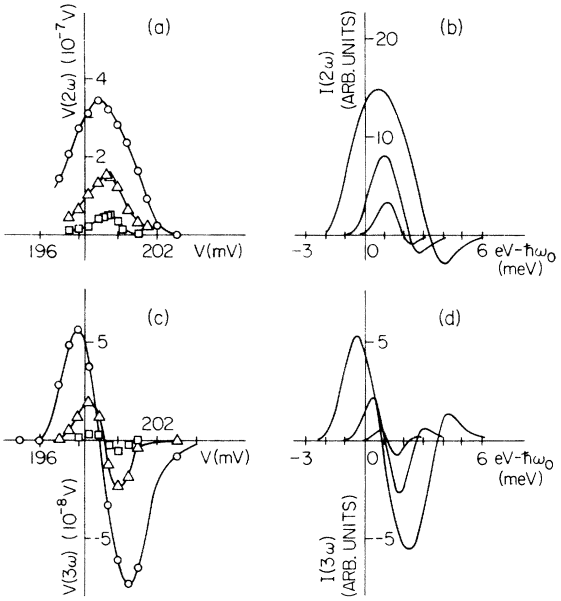

FIG. 3. Comparison of experimental and computer generated line shapes for an Al–Al-oxide–Pb junction at 1.1 °K for the second (a) and (b) and third (c) and (d) harmonic signals with three different modulation voltages. The vertical lines in (a) and (c) corresponds to the measured mode energy when the superconductivity was quenched with a magnet. The squares correspond to a 0.5-mV modulation, the triangles to a 1-mV modulation, and the circles to a 2-mV modulation. The width of the assumed Gaussian distribution of oscillator strengths was chosen to make the energy between the opposing peaks in the computed third harmonic signal fit experiment. For larger modulation voltages the signals get larger and broader and are shifted to lower energies. Note that although the computed and experimental curves match quite well in general the predicted tails in (b) and (d) are not present in the experimental plots (a) and (c).

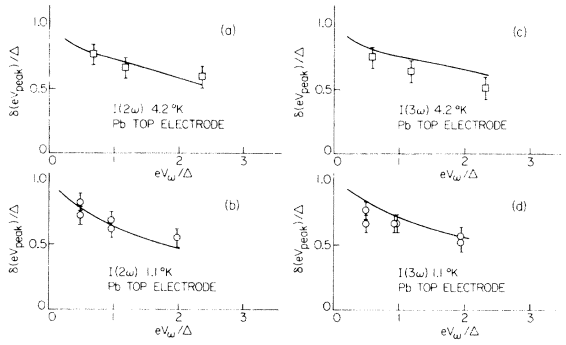

FIG. 4. Plot of predicted and experimental peak shifts $[\delta(eV_{peak})/\Delta]$ vs modulation voltage $[eV_\omega/\Delta]$ for the second and third harmonic signals of Al–Al-oxide–Pb junctions at 1.1 and 4.2 °K. The solid lines were computer generated as described in the text. Here $\Delta \equiv \Delta_{Al} + \Delta_{Pb}$ was measured from the elastic I-V characteristics of the junctions. For small modulation voltages the shift approaches Δ.

sponds to $eV_\omega = 1.414$ meV.) For larger modulation voltages the peaks get larger and broader and are shifted to lower energies. The width of the assumed Gaussian linewidth was chosen to make the energy spacing between peaks of the third harmonic signal agree with experiment. The best fit corresponded to a natural linewidth of 0.96 meV.

The agreement between the experimental and computer-generated curves is quite satisfying, in general. However, the computer-generated curves [Figs. 3(b) and 3(d)] have tails on the high-voltage side which correspond to the curvature introduced by the BCS density of states. These tails are markedly absent in the experimental curves [Figs. 3(a) and 3(c)]. We have as yet no explanation for this discrepancy.

Figure 4 shows computer-generated theoretical curves for the peak shifts (or zero-crossing shifts for the third harmonic signal) $\delta(eV_{peak})/\Delta$ due to superconductivity versus modulation voltage eV_ω/Δ for a Pb top electrode and an Al bottom electrode where $\Delta \equiv \Delta_{Pb} + \Delta_{Al}$, at 4.2° K, and 1.1° K. For comparison, the points are experimental measurements of the shifts produced when superconductivity was quenched with a magnetic field. The energy gaps were measured from the elastic current-voltage characteristics of the junctions. The curves agree well with experiment for the second harmonic signal. The third harmonic curve seems somewhat high, although still within a standard deviation of the experimental points.

The choice of width for the Gaussian distribution of oscillator strengths had very little effect on the predicted peak shifts until the widths were very much larger than the energy gap, at which point the shifts were decreased. However, since it was not possible to measure peak positions of very bread bands to the accuracy required to detect the added effect, we did not pursue this matter further.

IV. EFFECT OF TOP METAL ELECTRODE

Figure 2 shows a plot of the second harmonic signal versus applied voltage for the 198.3-meV C-C stretch mode of benzoic acid on alumina for Pb vs Ag top metal electrodes. The junction with the Ag top electrode has a peak that is shifted down by 0.4 meV with respect to that for the Pb top electrode with the superconductivity quenched. We studied the peak positions of five vibrational modes of benzoic acid on alumina for three different top metal electrodes. The modes studied (identified in Fig. 1) were chosen to give large and sharply defined peaks, a good spead in ener-

gies, and as many different types of vibrational modes as possible. Rather than quenching the superconductivity of the electrodes for all of our measurements, we obtained corrections for each type of junction for two vibrational modes, the ones at 198.3 and 143.3 meV, and used those corrections for the other mode energies measured with the films superconducting. This two-step procedure eliminated the need to cool the superconducting magnet for every run, thus saving a considerable amount of liquid helium.

The mean values of our measured peak positions, corrected for the shifts due to superconductivity, are presented in Table I. The standard deviation was approximately 0.1 meV for the molecular modes (the five modes below 200 meV) and approximately 1.5 meV for the O-D and O-H modes. The data can be summarized as follows: (i) Vibrational modes which involve little or no deformation of the C-H bonds (50.3, 76.3 and 85.0 meV) have mode energy shifts with different top metal electrodes too small to be measured with our techniques, (ii) the vibrational modes which involve deformation of the C-H bonds (143.3 and 198.3 meV) have shifts in their mode energies of order 0.5 meV; and (iii) the vibrational modes of the O-H and O-D ions on alumina have relatively large shifts, on the order of 14 meV.

The ordering with different top metals for the C-H bond mode shifts is the same as for the O-H and O-D bond shifts. Figure 5 plots the observed mode energies (after correction for the effects of superconductivity) against $1/R^3$, where R is the atomic radius of the top metal. As we argued in an earlier paper,[10] metals with smaller atomic volumes can pack more closely around

TABLE I. Vibrational-mode energies for Al–Al-oxide–benzoic-acid–metal IETS junctions.

Top metal [a]			Optical		
Ag	Sn	Pb	results	References	Assignment
50.2	50.3	50.3	50.1	21	δ(C-C)
76.4	76.4	76.3	76.5	22	β(C-C-C)
85.0	85.1	85.0	85.0	23	δ(C-C)
142.7	143.2	143.3	143.8	22	β(C-H)
197.9	198.1	198.3	198.5	22	ν(C-C)
327 [b]	330	333			ν(O-D)
438	444	446	455	24	ν(O-H)

[a] All peak energies are in meV. These values are the means of four or five measurements each. Standard deviations were approximately 0.1 meV for the molecular modes (the first five) and approximately 1.5 meV for the O-D and O-H modes.

[b] Measurements of O-D and O-H mode energies were made with no benzoic-acid dopant, as described in Ref. 10.

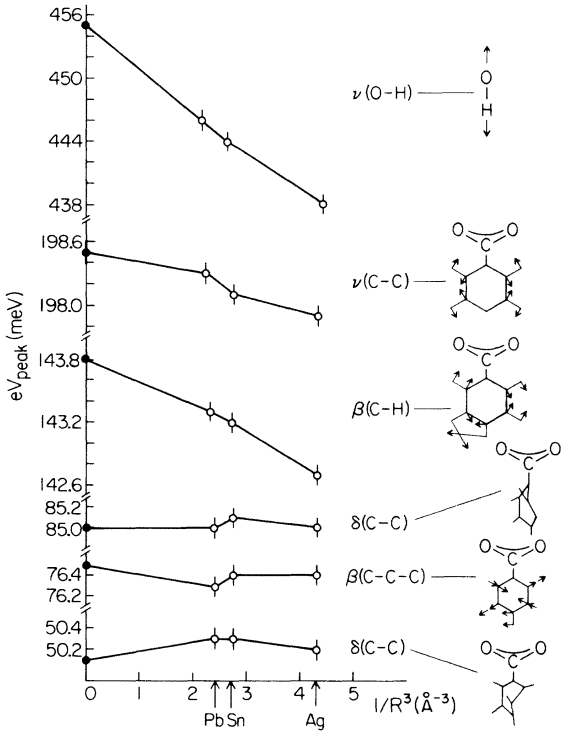

FIG. 5. Plot of measured peak positions of various modes of benzoic acid on alumina for different top metal electrodes vs $1/R^3$ (Å^{-3}), where R (Å) is the atomic radius of the top metal in angstrom units. The open circles are IETS measurements (with a top metal electrode) and the solid circles are optical measurements (without a top metal electrode). Those vibrational modes involving little deformation of the C-H bond have no measurable energy shifts. Those with appreciable C-H bond deformations (143.3 and 198.3 meV) have shifts of order 0.5 meV. The O-H stretching mode has a large shift of order 17 meV. Note that the scale is contracted by a factor of 10 for the O-H stretch mode.

dopant molecules and diffuse more easily into the tunneling barrier, reducing the effective distance between the oscillating dipole moment involved with a given vibration and the metal surface, increasing the image forces. Therefore metals with smaller atomic volumes produce larger downward shifts in the mode energies, as can be seen in Fig. 5. The solid points along the $1/R^3 = 0$ axis correspond to optical measurements of the corresponding mode energies on aluminum oxide. (The reasons for the choice of $1/R^3$ as the relevant variable will be discussed in Sec. V.)

V. IMAGE MODEL

A simple model for the effect of the top metal electrode assumes that the metal surface is planar and that an oscillating charge distribution located an equilibrium distance d from the metal induces

an image of itself in the metal surface. The interaction between the charge and its image modifies both the resonant frequency and the linewidth. We recognize, of course, that the surface is not planar on the scale of angstroms as we assume, but we hope to obtain the general behavior of the system from this model.

As pointed out in Sec. I, the image model has been worked out in detail by several authors. For our experiments the oscillating charge has a frequency ω_0 much less than the plasma frequency. Also, the phase shift on reflection of the incident radiation is very close to π.[25] In this limit the results of Kuhn,[3] Tews,[7] Chance, Prock, and Silbey,[8] and Morawitz and Philpott[9] reduce to those of the first work by Morawitz.[2]

The natural linewidths for our modes were smaller than the instrumental linewidths and difficult to unfold from experiment. Furthermore, we expect the effect of the top metal on the linewidth to be much smaller than its effect on the peak position.[9,10] We will therefore discuss only peak shifts.

In our earlier work[10] we introduced an image model in which the charge distribution associated with a vibrational mode was represented by a single charge q oscillating around an equilibrium point. This model is somewhat oversimplified in that the permanent dipole moment of a bond can be appreciably different from the dipole derivative of that bond.

In order to refine this model by accounting for both the static and oscillating dipole moments associated with a particular mode, we consider a static dipole moment $\vec{p}_0 = \vec{a}q_0$, where a is the O-H bond length, plus an oscillating dipole moment of form $\vec{p} = q_1\vec{x}$. The fields reflected back by the metal surface for the dipole moment oscillating perpendicular to the surface of the metal are[8] (at the position of the dipole)

$$\vec{E}_\perp = -\frac{2q_1 x n_1 \omega_0^3}{c^3}\left(\frac{1}{\gamma^3} - \frac{i}{\gamma^2}\right)e^{i\gamma}\hat{z} - \frac{q_0}{\epsilon}\left(\frac{1}{(2d)^2} - \frac{1}{(2d+a)^2}\right)\hat{z}. \tag{3}$$

Here n_1 is the real index of refraction of the oxide, ω_0 is the unperturbed frequency of oscillation, x is the displacement from equilibrium, and $\gamma = 2n_1\omega_0 d/c$, where d is the equilibrium distance from the charge to the metal surface. For the charge oscillating parallel to the metal surface[2]

$$\vec{E}_\parallel = -\frac{q_1 x n_1 \omega_0^3}{c^3}\left[\left(-\frac{1}{\gamma} + \frac{1}{\gamma^3} - \frac{i}{\gamma^2}\right)e^{i\gamma}\right]\hat{e}_\parallel - \frac{q_0}{\epsilon_1}\left(\frac{1}{(2d)^2} - \frac{1}{(2d+a)^2}\right)\hat{z}. \tag{4}$$

The force generated on the moving charge by these reflected fields is given by

$$\vec{F}_R = \mathrm{Re}\, q_1\vec{E}. \tag{5}$$

We treat the problem classically, using a Morse potential[26]

$$U(x) = E_D(1 - e^{-\beta x})^2, \tag{6}$$

Where E_D is the dissociation energy of the bond and β is defined by the relation $\omega_0^2 = 2\beta^2 E_D/m$, where m is the reduced mass of the bond pair.

Since in our experiments the wavelengths involved were a few microns while the distances are of the order of angstroms, we take the limit $\gamma \ll 1$. For $\vec{p}$ perpendicular to the surface we find

$$\Delta\omega_\perp = \frac{-q_1^2}{8m\omega_0 n_1^2 d^3}\left\{1 + \tfrac{3}{2}\beta\frac{q_0}{q_1}d\left[1 - \left(1 + \frac{a}{2d}\right)^{-2}\right]\right\}. \tag{7}$$

For p parallel to the surface,

$$\Delta\omega_\parallel = -q_1^2/16m\omega_0 n_1^2 d^3. \tag{8}$$

For typical dipole modes $3\beta d(q_0/q_1)$ is of order unity. Thus we see that the mode shifts for dipoles oriented parallel to the surface are smaller than the shifts for dipoles oriented perpendicular to the surface, but they are of the same order of magnitude. Note also that both shifts are proportional to $1/d^3$, where d is the effective distance to the metal plane.

Since d is not directly measurable, we used it as a variable to be fit with the observed peak shifts. For the O-H stretch mode at 446 meV, we assume $\vec{p}$ perpendicular to the surface and take $q_0 = 0.71e$,[27] $q_1 = 0.32e$,[27] $m = m_p$, $n_1^2 = 3$,[28] $\beta = 1.6 \times 10^8$ cm^{-1},[26] and find $d = 0.61$, 0.73 and 0.80 Å for Ag, Sn, and Pb top metal electrodes, respectively. Thus physically reasonable values of d will account for the observed mode shifts in the O-H mode. These values for d are somewhat smaller (~50%) than those obtained previously[10] because of the refinement of our model, and are perhaps an improvement in that they are closer to an atomic radius. Furthermore, as noted and discussed previously,[10] metals with larger atomic radii have larger effective d's.

There is some question as to where the effective imaging plane should be with respect to the metal surface. Newns[29] gives a simple expression in which the effective image charge is pushed back from the surface by a factor of $2\lambda^{-1}$, where λ^{-1} is the Fermi-Thomas screening length. Lang and Kohn[30] do a more involved calculation in which the image is shifted forward from the surface by roughly the same factor. In this paper we use the effective-charge–to–image distance as an adjust-

able parameter and argue that the values found ($2d \simeq 1.6$ Å) are not unreasonable.[31]

Let us now turn our attention to the C-H bend modes. The major difference between the C-H and the O-H modes is that the C-H dipole derivative is smaller: $q_1 \approx 0.1e$,[34] rather than $0.3e$. However, the energy of the C-H bend modes, $\hbar\omega_0$, is smaller by a factor of roughly 3. In addition here is only a small permanent dipole moment from the C-H bond. Finally, the C-H bend modes we studied are as much parallel as perpendicular to the surface. Thus if we assume that the effective distance d of the metal plane from the C-H modes is the same as for the O-H modes we would expect a ratio of the C-H mode shifts to the O-H mode shifts of $\lesssim 0.03$. In fact, these ratios were 0.03 ± 0.01 for the mode near 198 mV and 0.06 ± 0.01 for the mode near 143 mV. We regard this as surprisingly good agreement, considering the crudeness of the approximations used. Furthermore, the trend is the same as for the O-H mode shifts; metals with smaller atomic radii produced larger shifts.

Finally, let us consider C-C ring stretch and bend modes. One major difference between these modes and the C-H and O-H modes is that d should be larger. These modes primarily involve relative motion of carbon atoms within the ring. If we supposed that the appropriate d was thus increased on the order of 1 Å (a C-H bond length) the $1/d^3$ dependence of the mode shifts would reduce the C-C shifts by a factor of roughly 10. Furthermore, the effective mass is larger by a factor of 6, and q_1 is again only of order $0.1e$. Thus we would expect the ratio of these shifts to the O-H shifts to be of order 5×10^{-4}; that is, shifts less than 0.01 mV. This is well below our resolution of 0.2 mV. Indeed, we observed no shifts to within our resolution. This is gratifying, since such modes are extremely useful for compound identification by vibrational analysis.

In conclusion, the vibrational mode energies of adsorbed molecules as measured by inelastic electron tunneling spectroscopy, after correction for the effects due to the superconductivity of the electrodes, are shifted down in energy because of the presence of the top metal electrode. The shifts are in most cases not large enough to seriously effect the usefulness of IETS as a tool for the study of surface chemistry. Although it is not yet possible to eliminate hydrogen bonding between the included molecules and the top metal electrode as a possible contributing factor,[10] the absolute and relative magnitudes of the shifts can be explained in terms of a simple image model.

ACKNOWLEDGMENTS

We wish to thank Professor D. J. Scalapino for his help and encouragement throughout the course of this work. We also wish to thank Professor D. Cannell, Professor D. O. Harris, Professor R. C. Millikan, Professor D. Mills, and Professor W. E. Palke for valuable discussions, Professor R. C. Millikan for the use of his computer, and S. Tepper and K. Kirtley for programming assistance.

---

*Supported by NSF Grant No. DMR72-03276 A01.

[1]K. H. Drexhage, H. Kuhn, and F. P. Schaefer, Ber. Bunsenges. Phys. Chem. 72, 329 (1968).

[2]H. Morawitz, Phys. Rev. 187, 1792 (1969).

[3]H. Kuhn, J. Chem. Phys. 53, 101 (1970).

[4]G. Barton, Proc. R. Soc. A 320, 251 (1970).

[5]M. R. Philpott, Chem. Phys. Lett. 19, 435 (1973).

[6]P. Milonni and P. Knight, Opt. Commun. 9, 119 (1973).

[7]K. H. Tews, Ann. Phys. (N.Y.) 29, 97 (1973).

[8]R. Chance, A. Prock, and R. Silbey, J. Chem. Phys. 60, 2184 (1974); 60, 2744 (1974).

[9]H. Morawitz and M. R. Philpott, Phys. Rev. B 10, 4863 (1974).

[10]J. R. Kirtley and P. K. Hansma, Phys. Rev. B 12, 531 (1975).

[11]Benzoic acid reacts with the alumina to form a benzoate surface species (see Ref. 12).

[12]M. A. Simonsen, R. V. Coleman, and P. K. Hansma, J. Chem. Phys. 61, 3789 (1974).

[13]Good samples had roughly two orders of magnitude more resistance for doped junctions than for undoped junctions. Junctions with superconducting electrodes were evaluated by measuring the ratio of the conductivity at zero bias voltage to the conductivity at voltages above the superconducting gap voltage. This ratio was compared to theoretical predictions (Ref. 14) (e.g., $\frac{1}{7}$ for a Pb electrode at 4.2 °K). Junctions were rejected if the experimental ratio was larger than the theoretical prediction. In practice, fewer than 5% of our junctions were rejected by this criterion.

[14]See, for example, D. H. Douglass, Jr. and L. M. Falicov, in *Progress in Low Temperature Physics*, edited by C. J. Gorter (North-Holland, Amsterdam, 1964), Vol. 4, p. 114.

[15]We have found while writing this paper that this effect was first noted by Klein *et al.* (Ref. 17) during the preparation of their Fig. 11 [A. Legér (private communication)].

[16]J. Lambe and R. C. Jaklevic, Phys. Rev. 165, 821 (1968).

[17]J. Klein, A. Legér, M. Belin, D. Defourneau, and M. J. L. Sangster, Phys. Rev. B 7, 2336 (1973).

[18]J. Bardeen, L. N. Cooper, and J. R. Schrieffer, Phys. Rev. 108, 1175 (1957).

[19]δ-function, parabolic, and Lorentzian line shapes were also used. No significant differences in the predicted

peak positions were found, although slightly different line shapes were computed.
[20]Our numerical integration of Eq. (1) followed closely that of B. N. Taylor, Ph. D. thesis (University of Pennsylvania, 1963) (unpublished).
[21]J. H. S. Green, W. Kynaston, A. S. Lindsey, Spectrochim. Acta 17, 486 (1961).
[22]A. E. T. Kuiper, J. Medema, and J. J. G. M. van Bokhoven, J. Catal. 29, 40 (1973).
[23]S. Pinchas, D. Samuel, and M. Weiss-Broday, J. Chem. Soc. (Lond.), 2383 (1961).
[24]J. Schmidt (private communication).
[25]G. P. Motulevich, in *Optical Properties of Metals and Intermolecular Interactions*, edited by D. V. Skobel'tsyn [translated by O. D. Archard (Consultants Bureau, New York, 1973)], pp. 59–82.
[26]G. Herzberg, *Spectra of Diatomic Molecules* (Van Nostrand, New York, 1950).
[27]P. E. Cade, J. Chem. Phys. 17, 2390 (1967).
[28]P. W. Kruse, L. D. McGlauchlin, and R. B. McGuistan, *Elements of Infrared Technology: Generation, Transmission, and Detection* (Wiley, New York, 1963), p. 140.
[29]D. M. Newns, J. Chem. Phys. 50, 4572 (1969).
[30]N. D. Lang and W. Kohn, Phys. Rev. B 7, 3541 (1973).
[31]The image potential can be viewed as having its origin in the coupling of the exterior charge to surface plasmons (Refs. 32 and 33). If the external charge has a finite mass, recoil effects will cause a rounding of the image potential near the surface. However, for the parameters of the present problem the scale of this rounding is small relative to λ^{-1}. Thus the effects discussed in Refs. 29 and 30 are dominant.
[32]J. Sak, Phys. Rev. B 6, 3981 (1972).
[33]E. Evans and D. L. Mills, Phys. Rev. B 8, 4004 (1973).
[34]H. Spedding and D. H. Whiffen, Proc. R. Soc. A 238, 245 (1956).